

Theory of 2δ -kicked Quantum Rotors

C.E. Creffield,¹ S. Fishman,² and T.S. Monteiro¹

¹*Department of Physics and Astronomy, University College London, Gower Street, London WC1E 6BT, UK*

²*Physics Department, Technion, Haifa, IL-32000, Israel*

(Dated: October 1, 2018)

We examine the quantum dynamics of cold atoms subjected to *pairs* of closely spaced δ -kicks from standing waves of light, and find behaviour quite unlike the well-studied quantum kicked rotor (QKR). Recent experiments [Jones et al, *Phys. Rev. Lett.* **93**, 223002 (2004)] identified a regime of chaotic, anomalous classical diffusion. We show that the corresponding quantum phase-space has a cellular structure, arising from a unitary matrix with oscillating band-width. The corresponding eigenstates are exponentially localized, but scale with a fractional power, $L \sim \hbar^{-0.75}$, in contrast to the QKR for which $L \sim \hbar^{-1}$. The effect of inter-cell (and intra-cell) transport is investigated by studying the spectral fluctuations with both periodic as well as ‘open’ boundary conditions.

PACS numbers: 32.80.Pj, 05.45.Mt, 05.60.-k

I. INTRODUCTION

A recent experimental study [1] of cesium atoms subjected to pairs of near δ -kicks using pulsed optical potentials showed behaviour surprisingly different from the well-studied single-kick system, the quantum kicked rotor (QKR or δ -KR). The QKR is possibly the most studied experimental and theoretical paradigm of classical Hamiltonian chaos. The classical dynamics of the system make a gradual transition to chaotic dynamics as a function of an effective kick strength K (related to the intensity of the optical potential). It has also been well-investigated experimentally, using mainly cesium atoms [2]. In the large K (chaotic) regime, typical *classical* trajectories are diffusive; to lowest order, the diffusion is a random walk in momentum, with diffusion constant $D \approx \frac{K^2}{2}$. Then, for a corresponding ensemble of atoms, say, the average kinetic energy increases linearly with time i.e. $\langle p^2 \rangle / 2 \sim Dt$. Short-ranged correlations to the classical diffusion do exist, however, and their effects have also been observed experimentally [3].

In the corresponding quantum system, the quantum kicked rotor (QKR), the diffusion is arrested on a timescale $t^* \sim D/\hbar^2$. In experiments and calculations, an initially gaussian momentum distribution $N(p, t=0)$, is seen to evolve into an exponentially localized distribution $N(p, t > t^*) \sim \exp(-|p|/L)$, where $L \sim \frac{D}{\hbar}$. This quantum suppression of chaotic diffusion is an important quantum chaos phenomenon termed Dynamical Localization [4]. A formal connection between Dynamical Localization and Anderson localization, (the exponential localization of electronic wavefunctions in disordered metals) has been made [5].

Here we consider instead the case where the particles are subjected instead to *pairs* of closely spaced kicks: the 2δ -kicked rotor (2δ -KR). The recent experimental study [1] showed that the corresponding classical diffusion is anomalous, and involves many additional corrections from weak, but long-ranged (in time) correlations. The experiment identified periodically spaced

momentum-trapping regions where the atoms absorb little energy, interspersed by regions where they absorb energy even more rapidly than the standard δ -KR system.

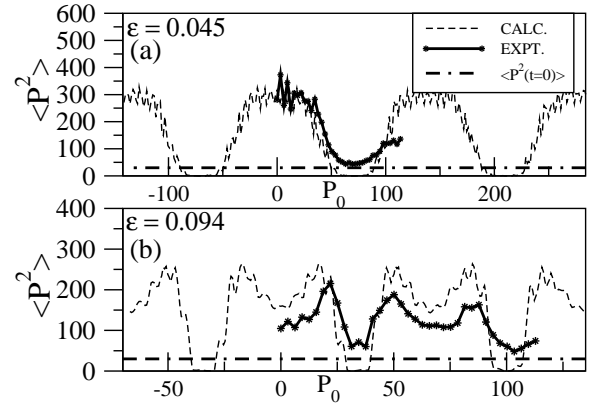


FIG. 1: Experimental results from [1] showing effects of momentum trapping. Each point indicates the energy absorbed by a cloud of cesium atoms after dynamical localization. The horizontal-axis gives the initial average momenta $\langle p \rangle = P_0$ of each cloud of cesium atoms: i.e. each atomic cloud initially has a gaussian momentum distribution well-centred on P_0 . The trapping regions correspond to $\langle p^2 \rangle \simeq 0$. All the data corresponds to effective values of $K = 3.2$ and $\hbar = 1$.

In this work we extend and develop a preliminary study of this system [6], and reveal unusual localization properties and spectral fluctuations not seen in the standard QKR. We find a novel dynamical localization regime, with generic localization lengths $L \propto \hbar^{-0.75}$ determined by a *fractional* exponent ($\simeq 0.75$). A similar exponent was found in $P(t) = |\langle \psi(t=0) | \psi(t) \rangle|^2 \sim t^{-0.75}$, the return probabilities. To our knowledge, there is no similar study of a KAM system so globally characterized by a single fractional exponent. A mixed phase-space regime (with a mixture of a chaotic regions and stable islands) can indeed exhibit fractional return probabilities [7], but it will typically have many competing exponents, characterizing only local regions of phase space. The quantum

localization properties are thus not generic, and depend sensitively on the detailed phase-space structure.

For the 2δ -KR, we present evidence indicating that the localization properties are related to the scaling properties of phase space in the vicinity of golden-ratio cantori. We argue that the observed behaviour is due to the presence of families of golden ratio cantori occupying an appreciable fraction of each cell. In addition, the ‘cellular’ momentum structure suggested by the experiments is shown to correspond to a time-evolution operator with a not previously investigated *periodically-oscillating* banded structure. The corresponding eigenstates can be well localized within a single cell defined by this oscillating band; or they may extend over several cells.

We characterize the spectral behaviour by two parameters: a filling parameter, R , which quantifies the fraction of a cell that a typical state occupies, and d , which quantifies inter-cell transport. We consider two types of distinct (but related) delocalization transitions: (a) a $0 \rightarrow 1$ cell transition as eigenstates fill one cell ($R \simeq 1$ but $d > 2$) (b) a $1 \rightarrow$ several cell transition, as states delocalize from a single cell to many, occurring for $R \gg 1$ and $d \leq 2$.

As the $0 \rightarrow 1$ cell transition occurs, all states extend into fractal cantori-filled regions bordering each cell; we identify a regime with spectral properties (particularly spectral variances which, while not identical, may be compared with ‘critical statistics’). The latter were first studied near the critical point of the Anderson Metal-Insulator transition (MIT) [8, 9, 10, 11, 12, 13]. So-called ‘critical statistics’ are now of much current interest in chaotic systems with classical discontinuities (non-KAM systems) [14, 15, 16, 17]; they have been attributed to the effect of cantori [16, 17]; however they are not expected in KAM system, due to their non-generic properties. Below, we use the term critical statistics in this broader sense, rather than specifically the critical point of the MIT.

Imposing periodic boundary conditions in momentum space effectively confines the system’s eigenstates to a single cell (with toroidal geometry). Such a calculation shows a transition from Poisson to Wigner-Dyson statistics (they are of similar functional form to GOE results, so are referred to as such below, although strictly they are COE statistics), via a new regime of intermediate statistics. We also calculate eigenstates for the open system (non-periodic boundary conditions). This calculation yields agreement with the single-cell calculation up to the onset of delocalization, but beyond shows rather different behaviour. For $d \simeq 2$ the spectral statistics show a signature of the onset of delocalization of the eigenstates into multiple cells, characterized by a return towards Poissonian statistics.

In summary, our main new results are 1) A study of the cellular form of the unitary operator of this system, which differs substantially with the behaviour of band random matrices (BRM), which approximate the ordinary QKR. 2) Numerical evidence for behaviour analo-

gous to critical statistics associated with cantori [17]. 3) The spectral signatures of delocalization from one cell, to several cells. 4) A novel regime of exponential localization determined by the fractional exponent 0.75, which coincides closely with the dominant scaling exponent obtained in the vicinity of golden-ratio cantori. In Section II, we review the present state of knowledge of the 2δ -KR. In Section III we introduce the time-evolution operator and obtain, for the first time, an analytical form for its bandwidth. In Section IV we investigate the dynamical localization and the fractional exponent $\nu = 0.75$. In Section V we look at the delocalization within a single cell, by solving the problem ‘on a torus’ in momentum space and compare with critical statistics. In Section VI we compare the behaviour with a calculation with ‘open’ boundary conditions and the signature for the onset of delocalization onto many cells. Finally in Section VII we give our conclusions and discussion.

II. THE 2δ -KR

We consider a system with a Hamiltonian corresponding to a sequence of closely spaced pairs of kicks:

$$H = \frac{p^2}{2} - K \cos x \sum_n [\delta(t - nT) + \delta(t - nT + \epsilon)],$$

where $\epsilon \ll T$ is a short time interval and K is the kick-strength. We now use a re-scaled time in units of T . The classical map for the 2δ -KR is then a two-kick map:

$$\begin{aligned} p_{j+1} &= p_j + K \sin x_j \\ x_{j+1} &= x_j + p_{j+1}\epsilon \\ p_{j+2} &= p_{j+1} + K \sin x_{j+1} \\ x_{j+2} &= x_{j+1} + p_{j+2}(1 - \epsilon). \end{aligned} \tag{2.1}$$

Clearly, the limit $\epsilon = 1$ or 0 corresponds to the Standard Map, which describes the classical dynamics of the QKR:

$$\begin{aligned} p_{i+1} &= p_i + K \sin x_i \\ x_{i+1} &= x_i + p_{i+1} \end{aligned} \tag{2.2}$$

An experimental realization of this system was obtained in [1], with cold cesium atoms in pulsed standing waves of light. Atoms with momenta $\langle p \rangle = p_0 \simeq (2m + 1)\pi/\epsilon$ (relative to the optical lattice) are confined in momentum trapping regions and absorb little energy; conversely, atoms prepared near $p_0\epsilon = 2m\pi$ experience rapid energy growth up to localization. The experimental trapping regions are shown in Fig.1. The basic mechanism of trapping is fairly intuitive: atoms for which $p_0\epsilon = (2m + 1)\pi$ and $m = 0, 1, \dots$ experience an impulse $K \sin x$ followed by another one $\simeq K \sin(x + \pi)$ which in effect cancels the first. Over time, however, there is

a gradual de-phasing of this classical ‘anti-resonant’ process. A theoretical study of the classical delocalization over longer times than a couple of kicks in [1] found anomalous momentum diffusion for all p_0 , with long-ranged corrections to the $D \simeq K^2/2$ uncorrelated diffusion rate, not present in the Standard Map.

Below we present the corresponding quantum behaviour.

III. TIME-EVOLUTION OPERATOR FOR 2 δ -QKR

The time evolution operator for this system may be written:

$$\hat{U}^\epsilon = \exp -i \frac{\hat{p}^2(T - \epsilon)}{2\hbar} \exp i \frac{K}{\hbar} \cos x \quad (3.1)$$

$$\exp -i \frac{\hat{p}^2 \epsilon}{2\hbar} \exp i \frac{K}{\hbar} \cos x$$

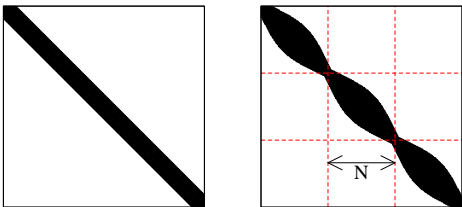


FIG. 2: Left (a): Structure of time-evolution matrix for a Quantum Kicked Rotor (QKR), in a basis of momentum states, showing the constant bandwidth structure typical of a Band Random Matrix (BRM). Right (b): Form of U^ϵ for our system, the 2 δ -QKR, showing the oscillating bandwidth structure. Before delocalization, eigenstates are confined within a single ‘momentum cell’ of dimension N .

In a basis of plane waves, \hat{U}^ϵ has matrix elements:

$$U_{lm}^\epsilon = U_l^{free} \cdot U_{lm}^{2-kick} = \exp -i \frac{l^2 \hbar (T - \epsilon)}{2} i^{l-m} \quad (3.2)$$

$$\sum_k J_{l-k} \left(\frac{K}{\hbar} \right) J_{k-m} \left(\frac{K}{\hbar} \right) e^{-i \frac{k^2 \hbar \epsilon}{2}}$$

where the $J_n(\frac{K}{\hbar})$ are integer Bessel functions of the first kind. It is easy to see that U_{lm}^{2-kick} is invariant if the products $K_\epsilon = K\epsilon$ and $\hbar_\epsilon = \hbar\epsilon$ are kept constant; while the free propagator $U_l^{free} = e^{-i \frac{l^2 \hbar (T - \epsilon)}{2}}$ simply contributes a near-random phase. Provided that $l^2 T \hbar \gg 2\pi$, the results are quite insensitive to the magnitude of $(T - \epsilon)\hbar$. Hence we often find it useful to consider the two scaled parameters K_ϵ and \hbar_ϵ , rather than to vary K, ϵ and \hbar independently.

The result in Eq.(3.2) may be compared with the one-kick map in Eq.2.2

$$U_{lm}^{(0)} = \exp -i \frac{l^2 T \hbar}{2} J_{l-m} \left(\frac{K}{\hbar} \right). \quad (3.3)$$

The one-kick matrix for the QKR has a well-studied band-structure: since $J_{l-m}(x) \simeq 0$ for $|l - m| \gg x$, we can define a bandwidth for $U^{(0)}$, namely, $b = \frac{K}{\hbar}$ (this is strictly a *half*-bandwidth) which is independent of the angular momenta l and m . However, this is *not* the case for the matrix of U^ϵ .

It is shown in the Appendix that, assuming $|l - m|$ is small, we can write:

$$U_{lm}^\epsilon \approx e^{-i\Phi} J_{l-m} \left(\frac{2K}{\hbar} \cos[l\hbar\epsilon/2] \right) \quad (3.4)$$

where the phase $\Phi = \frac{\hbar}{2}[l^2 T + \epsilon l m + \epsilon l^2] + \pi(l - m)/2$. Hence we infer a momentum dependent bandwidth, $b(p) = \frac{2K}{\hbar} \cos p\epsilon/2$. Fig.2 shows the calculated form of both matrices (white denotes matrix elements less than a small threshold). While $U^{(0)}$ has a constant bandwidth, the bandwidth for the matrix of U^ϵ oscillates with l from a maximum value $b_{max} = \frac{2K}{\hbar}$, equivalent to twice the bandwidth of $U^{(0)}$, down to a minimum value $b_{min} \sim 0$.

In effect, since $b_{min} \sim 0$, U^ϵ is partitioned into sub-matrices of dimension $N = \frac{2\pi}{\epsilon\hbar}$ corresponding precisely to the momentum cells of width $\Delta p = N\hbar$ observed in the experiment.

For the QKR, the localization properties of the eigenstates have been investigated extensively (see e.g. [20] for a review). The eigenstates are exponentially localized, with momentum probability distributions $N(p) \sim \exp -2|p|/L$, where the localization length $L \approx \frac{K^2}{4\hbar} = b^2 \hbar/4$, in the large K , small \hbar limits.

For the 2 δ -QKR, in the limit of small bandwidth $\frac{2K}{\hbar} \ll N$ we define a ‘local’ localization length for the eigenstates:

$$L(p) = b^2(p)\hbar/4 = \frac{K^2}{\hbar} \cos^2 p\epsilon/2 \quad (3.5)$$

This corresponds quite well with the oscillations seen in the experiment in Fig.1(a); the energy oscillates sinusoidally from a maximum value $\langle p^2 \rangle \simeq 400 \sim 4L^2 \simeq 4K^4$ for $K = 3.2$, $\hbar = 1$, (in re-scaled units) down to a minimum value $\langle p^2 \rangle \simeq 0$ for $P_0 \simeq \pi/\epsilon$. In contrast, Fig.1(b) corresponds to a regime where the eigenstates are tending to fill each cell, i.e. $L(p) \rightarrow N\hbar$.

In [18, 20] it was shown that the eigenstates of the QKR can also be obtained using a $U^{(0)}$ matrix of *finite* dimension N . The ratio of the localization length to N , was used to characterize the degree of ‘filling’ of the matrix $U^{(0)}$. It was shown that for a ratio $R \ll 1$ the behaviour is Poissonian. With increasing R , a transition to GOE behaviour was observed.

For the 2 δ -QKR we can also introduce a ‘filling factor’ R defined by the ratio [18]:

$$R_\epsilon = \frac{K^2}{N\hbar^2} = \frac{K_\epsilon^2}{2\pi\hbar_\epsilon}. \quad (3.6)$$

While for the 2 δ -QKR we have a natural choice of N , determined by the position of physical boundaries (the

trapping regions), the value of N in the QKR case is quite arbitrary. The problem is solved ‘on a torus’ in momentum. The momentum periodicity of the matrix is adjusted by a choice of a rational value of the kicking period $T\hbar$ (see Sec. V below). We can then compare matrices for both $U^{(0)}$ and U^ϵ , with similar N and R .

The interesting aspect of the 2δ -QKR system is that, as we show below, we can vary the coupling between the cells independently (with some constraints on allowable parameters) from the degree of filling of each individual cell. We will show below, that there is a particularly interesting regime where, for most eigenstates, $L(p) \sim N\hbar$, but the states are still largely trapped within a single cell. We can then ‘open’ the boundaries of the cells and investigate the delocalization regime.

In order to investigate the transport between cells, we examine the surprisingly different (relative to the QKR) process of dynamical localization in the 2δ -QKR.

IV. DYNAMICAL LOCALIZATION

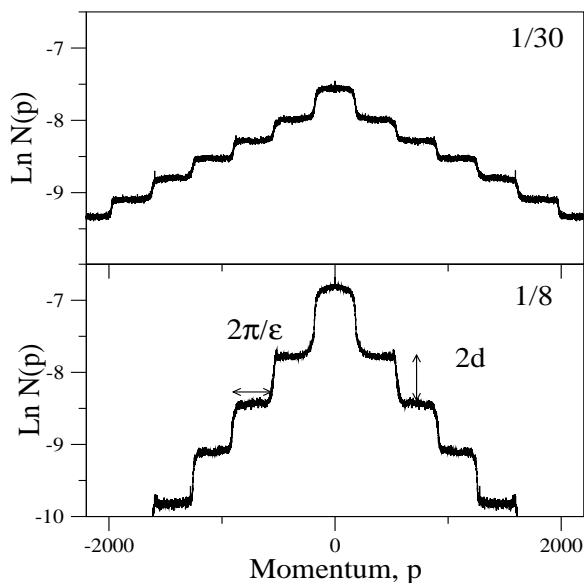


FIG. 3: Typical momentum distributions, $N(p)$, found after dynamical localization, for quantum wavepackets of the 2δ -QKR. Here $K = 20$, $\epsilon = 0.0175$ and $\hbar = 1/8$ and $1/30$ respectively. The $N(p)$ of the 2δ -QKR (slightly smoothed; for both eigenstates and wavepackets), show a long-range tail of ‘staircase’ form which on average follows the exponential $N(p) \sim \exp -2(p - \bar{p})/L_p$ where $L_p/2 = N\hbar/2d$; since $N\hbar = 2\pi/\epsilon$, the \hbar -dependence of L_p is determined by the drop in probability, d , at each cell boundary.

A set of wavepackets (all initially with $N(p, t = 0) \simeq \delta(p)$) were evolved in time, using the time evolution matrix U^ϵ , for a range of K , ϵ and \hbar . Fig.(3) shows typical momentum distributions obtained after a long time (beyond the ‘break-time’ t^* for the onset of dynamical localization). Fig.3 shows some typical momentum dis-

tributions $N(p)$. They are modulated by an exponential envelope

$$N(p) \sim \exp -\frac{2(p - \bar{p})}{L_p} \quad (4.1)$$

but with a regular ‘staircase’ structure superposed. There is a steep drop in probability at each step:

$$N^+(p) = \exp -2d N^-(p), \quad (4.2)$$

where $N^\pm(p)$ denote the probability after and before the step respectively. The localization length is

$$L_p = \frac{2\pi}{d\epsilon}. \quad (4.3)$$

The parameter d controls the transport through the cell boundaries. It also contains the \hbar dependence of L_p . In Fig.4, the dependence of d on $K\epsilon$ and $h_\epsilon = \hbar\epsilon$ is shown. It may be seen that to very good accuracy:

$$d \propto \frac{(\hbar\epsilon)^{0.75}}{f(K\epsilon)} \quad (4.4)$$

where $f(K\epsilon)$ is some function of $K\epsilon$. A rough fit yields an estimate, to within 50% or so:

$$d \simeq \frac{3.5(\hbar\epsilon)^{0.75}}{K_\epsilon^3}. \quad (4.5)$$

Hence we obtain the surprising result that for the 2δ -QKR, the localization length has an \hbar dependence with a fractional power, $L_p \sim \hbar^{-0.75}$. In comparison, for the QKR, $L_p \sim \hbar^{-1}$.

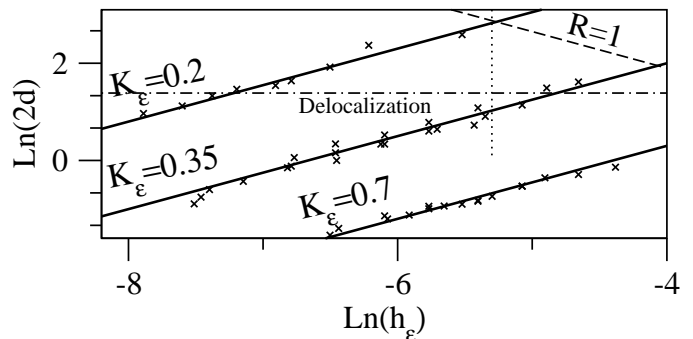


FIG. 4: Figure shows that $\text{Ln}(2d)$ plotted against $\text{Ln}(\hbar\epsilon)$ lies close to straight lines of invariant $K_\epsilon = K\epsilon$, with constant slope ≈ 0.75 . Hence $d \propto (\hbar\epsilon)^{0.75}$ and $L_p \propto \hbar^{-0.75}$ -in contrast to the well-known QKR result $L_p \propto \hbar^{-1}$. The dashed line indicates $R \simeq 1$ the one-cell filling border (i.e. $R > 1$ below the line). The *delocalization* border ($d \simeq 2$) is the dot-dash line (i.e. $d < 2$ below the line and represents the onset of significant coupling between cells). Statistics are presented later, in Fig.13, for points corresponding to the dotted line.

It is interesting to consider the origin of the $\hbar^{-0.75}$ behaviour. In fact, the first $\sim 1 - 2$ steps of the staircase can be seen in experiments with optical lattices of [1].

An earlier experiment [21] with pairs of broad pulses (as opposed to pulses short enough in duration to approximate δ -kicks) also showed a steep drop in probability over a narrow momentum region. This was identified as due to the presence of cantori. The finite pulse system does not have the momentum periodicity (and hence the generic character) of the 2δ -kicked system, and is effectively integrable at large p . Nevertheless, the classical dynamics is similar to the 2δ -QKR for $p \sim 0$. The QKR shows analogous behaviour: for pulses of finite duration, the classical dynamics is similar to the δ -kicked system for p small.

We can examine the classical behaviour in the trapping regions. Starting from the two-kick map Eq.2.1 and expanding our initial momenta around the trapping momenta $p_j \simeq P_n + \delta p^j$ where $P_n = (2n + 1)\pi/\epsilon$, we can write

$$p_{j+2} = p_j + K \sin x_j + K \sin [x_j + (2n + 1)\pi + \delta p^j \epsilon + K \epsilon \sin x_j]. \quad (4.6)$$

We can expand the trigonometric expressions, making small angle approximations if we assume $\delta p^j \epsilon \ll 2\pi$ and $K\epsilon \ll 2\pi$. In the trapping regions we then obtain an approximate one-kick map

$$p_{j+2} \simeq p_j - K^2 \frac{\epsilon}{2} \sin 2x_j - K \delta p^j \epsilon \cos x_j \quad (4.7)$$

$$x_{j+2} \simeq x_j + p_{j+2} T \quad (4.8)$$

The small angle assumption $\delta p^j \epsilon \ll \pi$ constrains Δp , the effective width of the trapping region,

$$\Delta p \sim 1/\epsilon. \quad (4.9)$$

A study of the Poincaré surfaces of section (SOS) may be found in [28]. But in summary, at the centre of the trapping region, where $\delta p^j = 0$, only the $\sin 2x$ kick in Eq.4.7 is significant so the classical SOS shows structure very similar to a ‘period-doubled’ Standard Map with impulse $V'(x) = K_{eff} \sin 2x$ where $K_{eff} \simeq K^2 \frac{\epsilon}{2}$ and K_{eff} is an effective kick strength. However, further out within the trapping region, the SOS show that it is the $\cos x$ kick in Eq.4.7 which is dominant and the island structure is similar to that of a Standard Map with impulse:

$$V'(x) \simeq K \delta p^j \epsilon \cos x. \quad (4.10)$$

Given the importance of the $K\epsilon$ scaling seen in Fig.4 (rather than a $K^2\epsilon$ scaling) we suggest that the $K_{eff} \cos x$ form of Eq.4.7 determines the quantum behaviour. This implies that regions with:

$$K \delta p^j \epsilon \gg K^2 \frac{\epsilon}{2} \quad (4.11)$$

dominate transport. This will be the case if δp_j is large; from Eq.4.9, we deduce that this implies the criterion $K\epsilon \ll 1$. However, if $K\epsilon$ is too small, the phase space will be too regular. Hence, values of $K\epsilon \approx 0.1 - 0.3$ seem indicated.

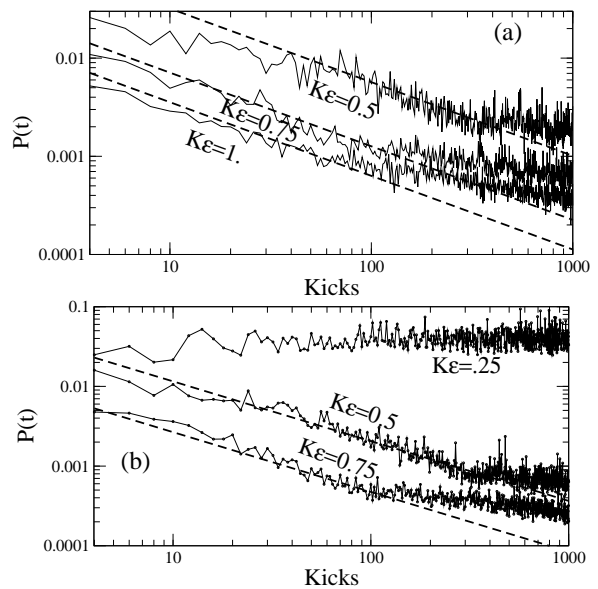


FIG. 5: Return probabilities for wavepackets prepared near the centre of the trapping regions indicating a $P(t) \sim t^{-0.75}$ decay, before localization. The dashed straight lines indicate a slope = 0.75. Note that at the lowest value of $K\epsilon = 0.25$, wavepackets prepared at the centre of the trapping region do not spread in momentum. (a) $\hbar = 1/8$ (b) $\hbar = 1/16$

In any case, the resonance structure in much of the trapping regions is always locally similar to the Standard Map, but with a varying effective kick strength (and phase of the impulse). For the Standard Map the last invariant phase-space manifolds correspond to $p/(2\pi) \simeq \phi$ or $\simeq 1 - \phi$ where ϕ is the Golden Ratio. The fractal remnant of this last manifold plays a role in transport in the Standard Map for $K \simeq 1 - 3$. Here, this would suggest $\delta p K \epsilon \approx 1 - 3$ and $\delta p \sim 10$.

The scaling properties of the phase-space around the golden ratio cantori were investigated by [24]. A characteristic exponent $\sigma_s \approx 0.75$ was found in directions dominated by elliptic fixed points. We term this the stable/dominant exponent. On the other hand $\sigma_u \approx .66$ was found in directions dominated by hyperbolic fixed points. We term this the unstable/sub-dominant exponent.

Previous studies of the QKR [23] found a $L \propto \hbar^{+\sigma}$ scaling, with $\sigma \simeq \sigma_u \simeq 0.66$, for momenta near the range $1 - \phi < pT/2\pi < \phi$. In [25], a $L \propto \hbar^{+\sigma_u}$ scaling was associated to a tunneling type process (termed ‘retunneling’) in [25]. An abrupt change to a regime with $L \propto \hbar^{-\sigma}$, with $\sigma \approx 0.5$, was also observed, and was attributed to a localization process which dominates when transport through the fractal cantoral regions is more ‘open’. In that work, it was argued that the process has similarities with dynamical localization.

The 2δ -KR results, with a negative sign on the exponent $L \sim \hbar^{-0.75}$ correspond to a localization regime, and are consistent with quantum probability ‘sticking’ mostly

to directions where there are (or were, at lower K) elliptic fixed points. One might speculate why no previous studies uncovered a regime dominated by σ_s ; we note that in [23, 25] the $L \sim \hbar^{+0.66}$ scaling refers to a local region; these are regimes where there are many stable islands and overall diffusion in each phase-space manifold is either absent, or rather slow. Here, in contrast, part of phase-space is taken by very chaotic, fast diffusing regions, with trajectories which roam freely over large areas of phase-space; the only appreciable localization occurs at the stabler parts of cantoral remnants. In many regimes, there can be contributions from $\sim 1/\epsilon$ groups of golden-ratio cantori, rather than simply a single region near $p/2\pi \simeq \phi$ like the Standard Map. We note that Fig.13 in [25], where the $\sigma = 0.5$ scaling is obtained, is in a difficult numerical regime: barring one data point, a value $\sigma \simeq 0.75$ is not implausible.

We also calculated return probabilities $P(t)$ of the quantum wavepackets with time, averaged over 100 initial starting conditions close to the centre of the trapping region,

$$P(t) = (1/100) \sum_{l_1}^{l_2} \langle P_l(t) \rangle, \quad (4.12)$$

where $P_l(t) = |\langle \psi(t) | \psi_l(t=0) \rangle|^2$. The initial condition was taken to be an angular momentum eigenstate $\psi_l(t=0) = |l\rangle$. The results were averaged from $l_1 = \pi/\epsilon\hbar$ to $l_2 = l_1 + 100$. Fig.5 shows plots of $P(t)$, which show that $P(t)$ decays as $t^{-0.75}$ up to the break-time. For the lowest values of $K\epsilon$, the $t^{-0.75}$ decay is not apparent since the wavepacket localizes almost immediately.

A well-known relation between power-law return probabilities and the spectral statistics (variances) has been investigated for ‘critical statistics’ in non-KAM billiards or the Anderson transition [9, 11, 13, 17]. While the present systems has important differences (it is a smooth KAM system; it has a cellular structure and an oscillating band unitary matrix), the pre-eminence of the single fractional exponent motivates an investigation of the spectral properties.

We investigate the statistics as a function of the filling factor R and the inter-cell transport parameter d . Calculations were done for two types of boundary conditions: periodic boundary conditions and ‘open’ (non-periodic) boundary conditions. These are discussed in turn below.

V. EIGENSTATES: PERIODIC BOUNDARY CONDITIONS

We may keep the dimension of the unitary matrix U to a finite value N by making the momentum periodic with period $N\hbar$, following the approach in [18, 19, 20]. In order to preserve unitarity we must use a resonant value of $\hbar\epsilon$. We take:

$$\hbar\epsilon = \frac{2\pi}{N} \quad (5.1)$$

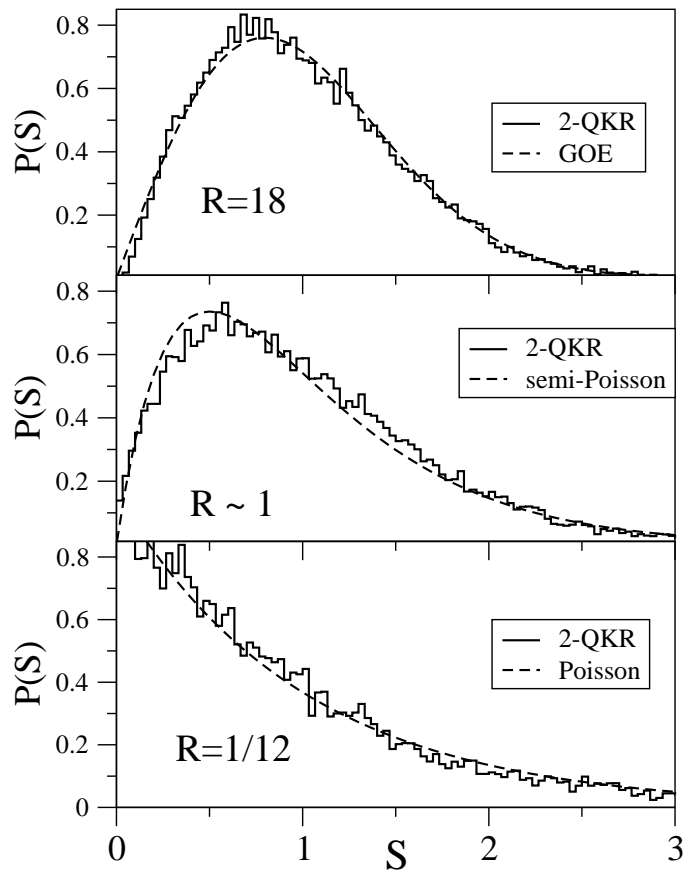


FIG. 6: Typical nearest-neighbour distributions $P(s)$, for periodic boundary conditions, for the $2\delta - KR$ as a function of the filling factor R . The distributions are Poissonian for small R , intermediate for $R \sim 1$ and GOE for sufficiently large R . Although the intermediate case never exactly follows the semi-Poisson distribution ($P(s) = 4se^{-2s}$), a comparison is useful, and so is shown in the middle figure

and then

$$\hbar\tau = \hbar(T - \epsilon) = M\hbar\epsilon \quad (5.2)$$

where M is the closest integer to $(T - \epsilon)/\epsilon$. We then construct a unitary matrix with elements:

$$U_{ln}(\tau_j) = \frac{1}{N} \exp -i\tau_j(l + \theta_x)^2/2 \sum_{k=-N_1}^{N_1} \exp i\frac{K}{\hbar} \cos 2\pi(k + \theta_p) \exp 2\pi i(k + \theta_p)(l - n) \quad (5.3)$$

We may have $\tau_1 = \hbar\epsilon$ or $\tau_2 = m\tau_1$. Here $N_1 = (N - 1)/2$. We construct the full two-kick matrix of dimension N

$$U_\epsilon(N) = U(\tau_1) U(\tau_2), \quad (5.4)$$

which is then diagonalized to obtain N eigenvalues and eigenstates. We may compare the results with the QKR

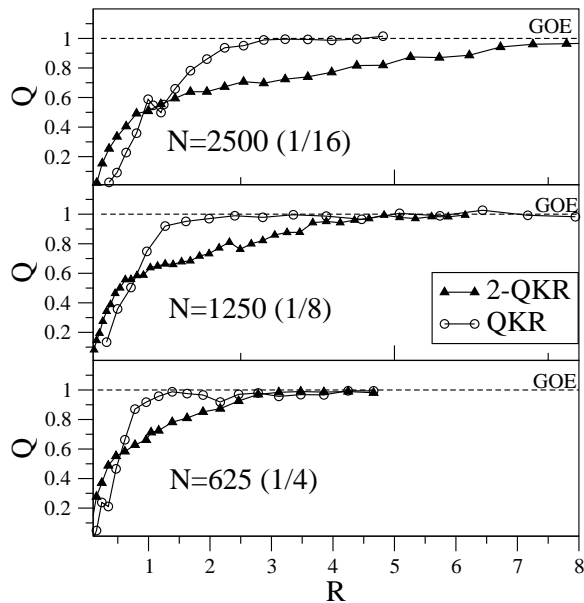


FIG. 7: Comparison of the transition from Poissonian ($Q = 0$) to GOE ($Q = 1$) NNS statistics for the QKR relative to the $2\delta - KR$ as a function of the filling factor $R = K^2/N\hbar^2$. While the QKR makes a rapid transition from Poisson to GOE for $R \simeq 1$, the $2\delta - KR$ on the other hand, shows a clear change in slope where delocalization of the quantum eigenstates is hindered by the fractal cell borders. Here $M = 25$; the values shown in brackets are approximate values of $\hbar = 2\pi M/N$; to avoid commensurability of M and N , actual values of N used were 629, 1259 and 2513.

equivalent

$$U^0(N) = U(T\hbar). \quad (5.5)$$

Here $\hbar = 2M\pi/N$, where M is an integer (non commensurate with N) which determines the momentum width of the matrix, i.e. $N\hbar = 2M\pi$; unlike the 2δ -KR, there is no underlying physical cellular phase-space structure to justify the choice of a particular M, N .

Note the dependence of the matrix elements on two Bloch phases: θ_p is a Bloch phase in the p direction while θ_x , the Bloch phase in the x direction, is the quasi-momentum. If $\theta_p \neq 0, \pi$, parity is not a good quantum number and we may use all eigenvalues in the statistics, regardless of parity. It is customary (e.g. [7, 17]) to calculate spectra for several θ_p to improve significance. In practice, we found that for the $2\delta - KR$, even for sizable K , there are very localized states which are too removed from the boundaries and generate pairs of parity-related pairs of near-degeneracies. The parity conservation effect is more effectively eliminated by, in addition to $\theta_p \neq 0, \pi$, also having $\theta_x \neq 0, 0.5$. The cantori effects we investigate are not affected by a non-zero quasi-momentum, and thus we average over several quasi-momenta.

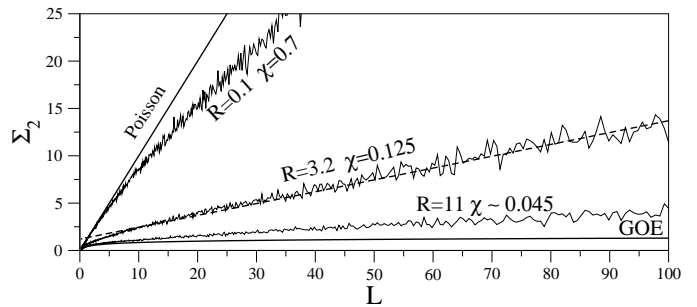


FIG. 8: Typical number variances $\Sigma_2(L)$ as a function of R for the $2\delta - KR$. We use the best fit to the slope to estimate the level compressibility χ . For R small, we have Poissonian statistics and $\Sigma_2(L) \simeq \chi L \simeq L$. For sufficiently large L , $\Sigma_2(L) \sim Ln(L)$ is far from linear; in this case the value $\chi < 0.05$ is simply an indication that $\Sigma_2(L)$ is close to the GOE limit. We identify an intermediate regime where $\Sigma_2(L) \sim \chi L$ for $1 \ll L \ll N$, (here $N = 2513$) with $\chi \sim 0.13$, corresponding to a similar range of R as the regime seen in Fig.7.

A. Effects of cantori in $0 \rightarrow 1$ cell transition: QKR versus $2\delta - KR$

We have calculated eigenvalues of the unitary matrix for a range of values of M, N and K . Below we compare nearest neighbour ($P(S)$) distributions and spectral variances $\Sigma_2(L) = \langle L^2 \rangle - \langle L \rangle^2$, of the $2\delta - KR$ with those of the QKR as a function of the filling factor $R = K^2/N\hbar^2$. We present results for $M = 25$ (i.e. $\epsilon = 0.04$) and values close to $N = 625, 1250$ and 2500 (one cannot have N, M commensurate).

In Fig.6 we show typical NNS distributions for $R \ll 1$, $R \sim 1$ and $R \gg 1$. For both single/double-kicked systems, the behaviour evolves from Poissonian to GOE, via an intermediate distribution at $R \sim 1$. While the $2\delta - KR$ does not exactly show the intermediate Semi-Poisson form, it can get quite close, and so a comparison is helpful. Here we quantify the deviation of $P(S)$ from $P_P(S)$ and $P_{GOE}(S)$, its Poisson and GOE limits respectively, with a quantity Q [26]:

$$1 - Q = \frac{\int_0^{S_0} (P(S') - P_{GOE}(S')) dS'}{\int_0^{S_0} (P_P(S') - P_{GOE}(S')) dS'}. \quad (5.6)$$

Hence $Q = 0$ indicates a Poisson distribution, while $Q = 1$ signals a GOE distribution. We take $S_0 = 0.3$. In Fig.7 we plot Q as a function of R . We find that while the QKR moves rapidly from Poisson to GOE for $R \sim 1$, the $2\delta - KR$ curve abruptly changes slope and the distribution evolves much more slowly towards GOE. We identify this as the regime where delocalization of the eigenstates over the whole cell is constrained by the cantori regions bordering the cells. A fit to alternative functions, such as the Berry-Robnik [27], gives a qualitatively similar picture.

In Fig.8, we show that the variances are close to Poissonian $\Sigma_2(L) \simeq L$ for small R , and are close to GOE

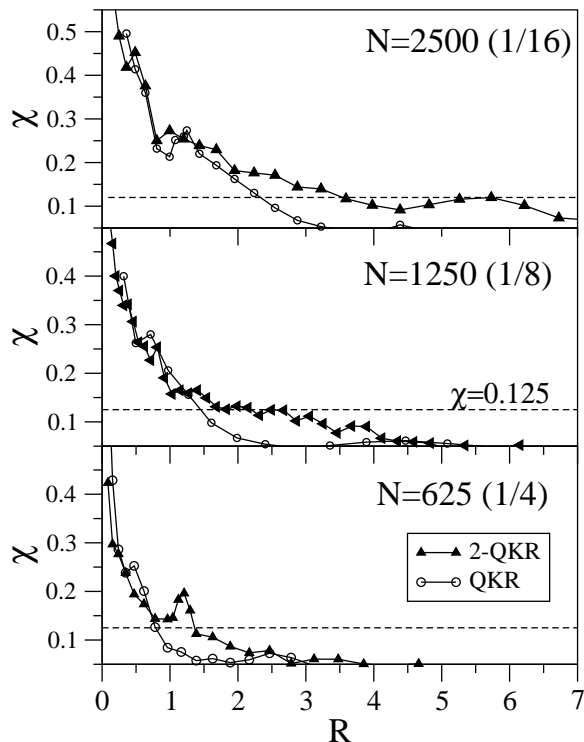


FIG. 9: Shows slopes (χ) of the variances $\Sigma_2(L)$. Figure compares the transition from Poissonian ($\chi = 1$) to GOE ($\chi < 0.05$) for the QKR with those of the $2\delta - KR$ as a function of the filling factor $R = K^2/N\hbar^2$. Parameters are similar to Fig7. The QKR makes a rapid transition to GOE at $R \simeq 1$ (with the exception of the small minimum seen at $R \simeq 1$ and $N = 2500$ which corresponds to a classical anti-resonance $K \simeq \pi$). The $2\delta - KR$ on the other hand shows an approximate plateau near $\chi \simeq 0.125$, the value one might expect from the ‘critical’ statistics relation $\chi \simeq 1/2(1 - D_2)$ if $D_2 \simeq 0.75$.

for large R . However, for $R \sim 1$ there is a regime, with nearly linear slope, $\Sigma_2(L) \simeq \chi L$ for $L \gg 1$ but $L \ll N$. We fitted the slopes of the $\Sigma_2(L)$ to the best straight line in the range $L = 7 \rightarrow 37$. We note that the graphs are not necessarily very linear everywhere: in certain regimes there is a pronounced curvature. Nevertheless, the procedure does give an indication of the average slope. While the $N = 2500$ results may remain linear out to $L \approx 100$, the $N = 625$ results saturate at much lower L , hence the $L = 7 - 37$ range is a compromise, good for all three cell sizes.

In Fig.9 we plot the slopes χ (the level compressibilities), for the 2δ -KR. We see that above $R \simeq 1$, there is, relative to the QKR, a plateau in the level compressibility, where $\chi \approx 0.12$. This behaviour is completely absent in the QKR: for $R \simeq 1$, the values of χ evolve rapidly towards the GOE limit.

We recall the results [9] for the level compressibilities of the Anderson MIT. It is predicted that asymptotically the variances have a linear form, for $L \gg 1$:

$$\Sigma_2(L) \approx \chi L, \quad (5.7)$$

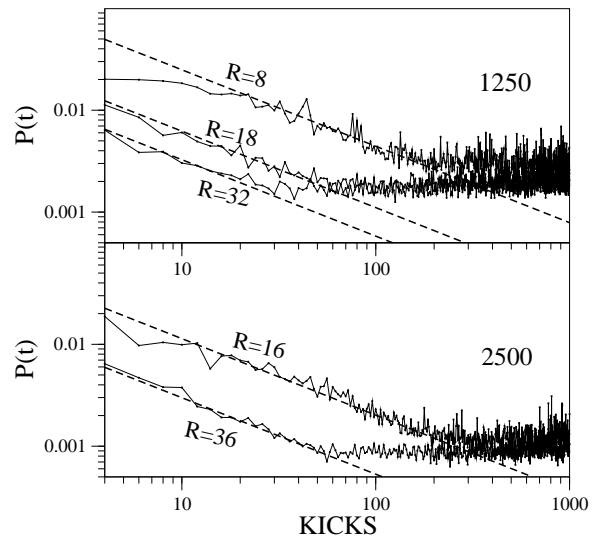


FIG. 10: Return probabilities for the finite dimensional problem, for similar parameters to Fig.5. The $P(t)$ still decay as $t^{-0.75}$ for $t < t^*$, but $P(t) \rightarrow 2/N$ for $t \rightarrow \infty$.

where

$$\chi \approx 1/2(1 - D_2/D) < 1 \quad (5.8)$$

and D is the spatial dimension. D_2 is a multifractal exponent related to the inverse participation ratio. This behaviour corresponds [9], in the MIT, to return probabilities which decay as $P(t) \sim t^{-D_2}$ and is considered a ‘fingerprint’ of critical systems, even in systems without disorder such as the non-KAM billiards [17].

Here we calculate the return probabilities using the eigenstates $|\alpha\rangle$ and eigenvalues $e^{i\omega_\alpha}$ of the N -dimensional matrix. We calculate

$$P_l(t) = \sum_l |e^{i\omega_\alpha} \langle l|\alpha\rangle|^2 \quad (5.9)$$

and average $P_l(t)$ over different starting conditions in the trapping regions $|l\rangle$, exactly as in Eq.4.12.

We note that in Eq.4.12, the $P(t)$ were obtained independently of the eigenstates by direct time evolution of a wavepacket in the *unbounded* system. The behaviour in Fig.10 is very similar to that in Fig.5, and again a decay rate $P(t) \sim t^{-0.75}$ is apparent. However, $P(t)$ in Fig.10 saturates to a larger value than for Fig.5, where the wavepackets are not restricted to a finite cell. For the finite N case $P(t) \rightarrow 2/N$ as $t \rightarrow \infty$ (the factor of 2 is attributed to weak localization [29]). We also observe that for $R \simeq 1$, in the regime with $\chi \sim 0.125$, wavepackets started in the trapping regions localize too rapidly to demonstrate the power-law decay. Nevertheless the behaviour of χ is -numerically- consistent with a fractal exponent $D_2 \simeq 0.75$.

We see here that $\chi \approx 0.125 = 1/2(1 - \nu)$ would imply $\nu \approx 0.75$, close to the exponent we obtained previously. This indicates that here ν , the dominant exponent near

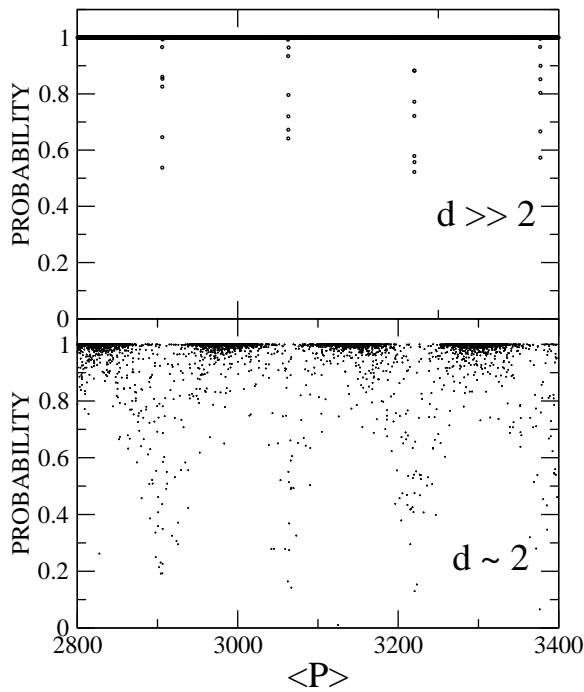


FIG. 11: Figure shows the effect of delocalization onto multiple cells: each point indicates the total probability of finding a given eigenstate in the cell which contains its average momentum $\langle p \rangle$. Well below the delocalization border, ($d \gg 2$) all states are fully contained in their assigned cell (barring a few edge-states at the boundary of each cell). But, at the ‘delocalization border’ ($d \sim 2$), a proportion of states have appreciable probability in neighbouring cells – in fact about 2% of states have less than half of their probability in their assigned cell. Results correspond to $\epsilon = 0.04, \hbar = 1/8$ and $K = 3$ (upper figure) or $K = 7$ (lower figure).

the golden-ratio cantori, may play a role equivalent to the multi-fractal exponent D_2 in the Anderson MIT. This is a significant result as such behaviour has not been seen and is not expected in a KAM system [16].

Unlike the billiard systems, here phase-space is not homogeneously filled with cantori. However, underlying classical trajectories may spend considerable time trapped within the fractal trapping regions which border the cell. The corresponding typical quantum states for $R > 1$ also sample the cantori region, but localize inhomogeneously in the fractal regions. As R increases, however, the distribution delocalizes into a more typically ergodic regime and the variances evolve towards the GOE ($\Sigma_2(L) \sim Ln L$) limit.

VI. OPEN BOUNDARY CONDITIONS: DELOCALIZATION FROM SINGLE TO MULTIPLE CELLS

We diagonalize the matrix of U^ϵ , with elements given by Eq.3.2 in a basis of a given parity, dimension $N_{TOT} = 10,000 \gg N$, for various K, ϵ and \hbar and obtain all eigen-

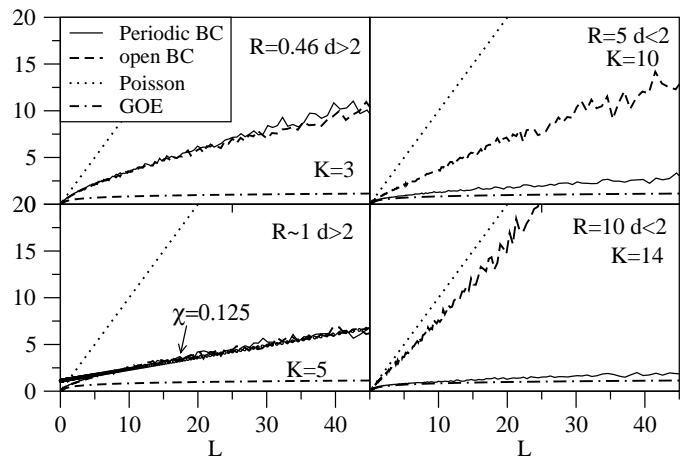


FIG. 12: Shows the effects of delocalization onto multiple cells on the spectral variances. Variances obtained with periodic boundary conditions ($N \approx 1250$) are compared with ‘open’ boundary conditions ($N_{tot} = 10,000, N \approx 1250, M = 51$). For $d > 2$, the eigenstates are well confined within a single cell and there is no significant difference between ‘open’ and ‘closed’ BCs. When $d < 2$, the results are sensitive to the BCs. While the ‘closed’ (periodic) BCs results tend to GOE, the ‘open’ results revert towards Poissonian statistics.

values and eigenvectors. For our calculations the cell dimensions are in the range $N \simeq 600 - 2500$ and hence each diagonalization spans N_{TOT}/N cells (fewer are kept since states in the cells at the edges of the matrix are discarded).

For instance results presented below have $\epsilon = 0.04$ and $\hbar = 1/8$. Hence, each cell contains $N = 2\pi/(\hbar\epsilon) \simeq 1257$ states so each diagonalization obtains up to 7 complete cells. Each full spectrum of length $N_{TOT} = 10,000$ is now split into 8 single cell sub-spectra. We assign the i -th eigenvalue to the m -th cell if

$$(2m-1)\frac{\pi}{\epsilon} \leq \bar{p}_i < (2m+1)\frac{\pi}{\epsilon}. \quad (6.1)$$

We calculate $P(S)$ and variances separately for each of these sub-spectra of length $N = 1257$. We then average the statistical distributions of 10-40 cells to obtain smoother distributions. We diagonalize U^ϵ for basis states between $l = 10,000 - 20,000$ as easily as states between $70,000 - 80,000$, for example, so as large a number of sets of 7 sub-spectra may be obtained as required. For the most delocalized spectra (with $K = 14$) only a single central cell of about 1250 states was sufficiently well converged to be used for statistics.

Fig.10 investigates how much of the momentum probability for each eigenstate is contained in the cell it was assigned to: for $R \leq 1$ and $d > 2$ the eigenstates are essentially fully contained within the cells they are assigned to. However, at the onset of delocalization, this procedure begins to fail; the expectation value \bar{p}_i of an eigenstate may assign it to the m -th cell; however, most of its probability may in fact be trapped in neighbouring

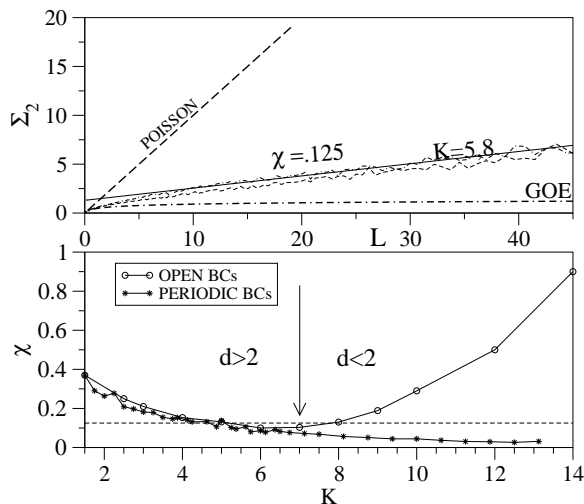


FIG. 13: Upper figure: shows that the variances (Σ_2 statistics) for open BCs can pass close to the so-called ‘critical’ regime of near-linear variances, with a slope close to $\chi \approx 0.125$. Lower figure: compares values of χ for ‘open’ BCs (a unitary matrix of dimension $N_{tot} = 10,000$ is diagonalized to obtain cells of dimension $N \approx 1250$) with ‘closed’ BCs (a finite matrix of dimension $N \approx 1250$, $M = 51$ is diagonalized, with periodic BCs to retain unitarity). The results are in excellent agreement before delocalization $d > 2$. After delocalization $d < 2$, the ‘closed’ BCs tend to GOE, the ‘open’ BCs tend to Poissonian behaviour, providing a clear signature of delocalization into multiple cells.

cells. This means that increasingly, the eigenvalues of the sub-spectra become uncorrelated and we can expect to see a return towards Poissonian statistics.

The apparent ‘failure’ of this procedure, in fact provides a good marker of delocalization from one-to-several cells. In contrast, the periodic boundary conditions presented in the previous section, could indicate only the degree of ‘filling’ of each single cell. Finally, we compare the spectral fluctuations for the two different types of boundary conditions (periodic vs open) in Figs.12-14. In Fig.12 and Fig.13 we show that the spectral variances are insensitive to the boundary conditions for $d > 2$. However for $d < 2$, the variances with periodic boundary conditions gradually make a transition to GOE behaviour, while the variances for the ‘open’ system begin to return back to Poissonian statistics. Fig.14 shows that the NNS distributions closely follow the same trends.

VII. CONCLUSIONS AND DISCUSSION

In conclusion, we have investigated the quantum behaviour of atoms exposed to pairs of δ -kicks and shown that the cellular structure arises from a novel oscillatory band structure of the corresponding unitary matrix. One consequence is a new type of localization-delocalization transition not seen in the QKR, where states delocalize from a single cell to many, associated with a character-

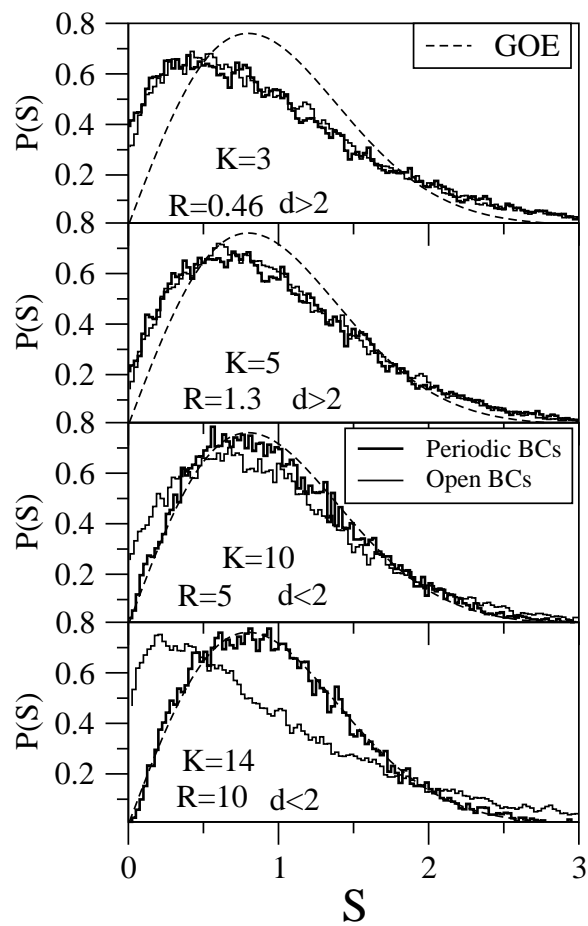


FIG. 14: Behaviour of NNS distributions equivalent to the results in Figs.12 and Fig.13. The results are insensitive to BCs before the onset of delocalization onto multiple cells $d > 2$. After delocalization $d < 2$, the ‘closed’ BCs yield GOE, the ‘open’ BCs tend to more Poissonian behaviour.

istic spectral signature (the return to Poissonian statistics).

We have also found certain scalings $L \sim \hbar^{-0.75}$ and $P(t) \sim t^{-0.75}$ which we argue result from the bands of cantori present on the borders of each cell. We argue also that the 0.75 exponent may be identified with the dominant stability exponent obtained previously near golden-ratio cantori. We show that the spectral fluctuations (both the NNS and spectral variances) show important differences with the QKR in regimes where the delocalization of eigenstates is hindered by cantori. The numerics provides evidence for behaviour somewhat analogous to ‘critical’ statistics of non-KAM billiards (in particular linear variances, with $\chi \approx 0.125$). These results are novel but important questions remain: while the $L \sim \hbar^{-0.75}$ dependence might be explained thus, it remains unclear why a similar exponent should also be found in the decay of the return probabilities $P(t) \sim t^{-0.75}$. The question of whether the $\nu = 0.75$ exponent is somehow equivalent to D_2 in the MIT and non-KAM billiards (in other words whether ν related to any underlying multifractal

character of the wavefunctions) remains to be addressed in future.

By implication, the study shows that the behaviour of cold atoms in double-pulsed standing waves of light is quite different from the single-pulsed systems. Some aspects were already identified in the experiments of [1] and may have applications in atom optics and atom chips, possibly as a mechanism for selecting atoms according to their momentum.

Acknowledgments

We are grateful to Phil Jones for the use of the experimental data in Fig.1. CEC and TM acknowledge support from the Engineering and Physical Sciences Research Council. We acknowledge the hospitality of the organisers of the workshop on "Resonances and Periodic Orbits: Spectrum and Zeta Functions in Quantum and Classical Chaos" at Institut Henri Poincare, Paris, in 2005. SF would like to thank Richard Prange and Edward Ott for the hospitality at the University of Maryland, where the work was completed.

APPENDIX A: DERIVATION OF THE APPROXIMATION (EQ.3.4) FOR U_{lm}^ϵ

In this Appendix Eq.3.4 will be derived for small ϵ . The crucial point in this derivation is that contributions to the sum in Eq.3.2 of terms where

$$|k - l| \gg K/\hbar \quad |k - m| \gg K/\hbar \quad (\text{A1})$$

are negligible. This implies that for terms that contribute appreciably, k is close to l and m . Therefore the corresponding operator $\hat{k} = \hat{p}/\hbar$ can be written in the form

$$\hat{k} = k_0 + \hat{k}_1 \quad (\text{A2})$$

where k_0 is a number close to l and m . Appreciable contributions to the sum are found only for

$$|k_1| \leq K/\hbar. \quad (\text{A3})$$

If $\hbar\epsilon(K/\hbar)^2 \ll 1$, as is the case for small ϵ , the condition $\hbar\epsilon k_1^2 \ll 1$ is satisfied, justifying the approximation

$$\exp -i\frac{\hat{p}^2\epsilon}{2\hbar} = \exp -i\frac{\hbar\epsilon\hat{k}^2}{2} \approx \exp -i\frac{\hbar\epsilon k_0^2}{2} \exp -i\hbar\epsilon k_0\hat{k}_1. \quad (\text{A4})$$

Substitution in Eq.3.1 with $\hat{k}_1 = -i\frac{\partial}{\partial x}$, and making use of the fact that $\exp -i\hbar\epsilon k_0\frac{\partial}{\partial x}$ is the shift operator, one finds

$$U_{lm}^\epsilon \approx e^{-i\frac{\hbar}{2}[(T-\epsilon)l^2 + \epsilon k_0^2]} \quad (\text{A5})$$

$$\langle l | e^{-i\frac{K}{\hbar}[\cos x + \cos(x - \hbar\epsilon k_0)]} e^{-i\hbar\epsilon k_0\hat{k}_1} | m \rangle,$$

that reduces to

$$U_{lm}^\epsilon \approx e^{-i\frac{\hbar}{2}[(T-\epsilon)l^2 + \epsilon k_0^2 + 2\epsilon k_0 m]} \quad (\text{A6})$$

$$\langle l | e^{-i\frac{2K}{\hbar}[\cos(x - \frac{1}{2}\hbar\epsilon k_0) \cos(\frac{1}{2}\hbar\epsilon k_0)]} | m \rangle.$$

The matrix element is calculated with the help of the identity

$$\frac{1}{2\pi} \int_{-\pi}^{\pi} dx e^{-i\beta \cos(x-\alpha)} e^{imx} = e^{im(\alpha-\pi/2)} J_m(\beta) \quad (\text{A7})$$

resulting in

$$U_{lm}^\epsilon \approx e^{-i\frac{\hbar}{2}[(T-\epsilon)l^2 + \epsilon k_0^2 + \epsilon k_0 m + \epsilon k_0 l]} \quad (\text{A8})$$

$$e^{i\frac{\pi}{2}(l-m)} J_{m-l} \left(\frac{2K}{\hbar} \cos \left(\frac{1}{2}\hbar\epsilon k_0 \right) \right).$$

Indeed appreciable contributions are found only for $|m - l| \lesssim 2K/\hbar$ in agreement with (A1). Since k_0 is close to l and m , within the approximation of this Appendix, it can be replaced by one of these. The substitution $k_0 = l$ results in Eq.3.4.

-
- [1] P.H. Jones, M. Stocklin, G. Hur, and T.S. Monteiro, Phys. Rev. Lett. **93**, 223002 (2004).
 - [2] F.L. Moore, J.C. Robinson, C.F. Bharucha, B. Sundaram, and M.G. Raizen, Phys. Rev. Lett. **75**, 4598 (1995).
 - [3] B.G. Klappauf, W.H. Oskay, D.A. Steck, and M.G. Raizen, Phys. Rev. Lett. **81**, 4044 (1998).
 - [4] G. Casati, B.V. Chirikov, F.M. Izraelev, and J. Ford, in "Lecture notes in Physics", Springer, Berlin, **93**, 334 (1979).
 - [5] S. Fishman, D.R. Grempel, and R.E. Prange, Phys. Rev. Lett. **49**, 509 (1982).
 - [6] C.E. Creffield, G. Hur, and T.S. Monteiro, preprint physics/0504074 (2005).
 - [7] R. Ketzmerick, L. Hufnagel, F. Steinbach, and M. Weiss, Phys. Rev. Lett. **85**, 1214 (2000).
 - [8] B.I. Shklovskii, B. Shapiro, B.R. Sears et al, Phys. Rev. B. **47**, 11487 (1993).
 - [9] J.T. Chalker, I.V. Lerner, and R.A. Smith, Phys. Rev. Lett. **77**, 554 (1996).
 - [10] B. Huckstein and L. Schweizer, Phys. Rev. Lett. **72**, 713 (1994).
 - [11] V.E. Kravtsov and K.A. Muttalib, Phys. Rev. Lett. **79**, 1913 (1997).
 - [12] D. Braun, G. Montambaux, and M. Pascaud, Phys. Rev. Lett. **81**, 1062 (1998).
 - [13] F. Evers and A.D. Mirlin, Phys. Rev. Lett. **84**, 3690 (2000); A.D. Mirlin Phys. Rep. **326**, 259 (1999).
 - [14] E.B. Bogomolny, U. Gerland, and C. Schmidt, Phys. Rev. E **59**, R1315 (1999).
 - [15] J. Wiersig, Phys. Rev. E, **65**, 04627, (2002).
 - [16] A.M. Garcia-Garcia and J.J.M. Verbaarschot, Phys. Rev.

- E.**67**, 046104 (2003).
- [17] A.M. Garcia-Garcia and J. Wang, Phys. Rev. Lett. **94**, 244102 (2005).
- [18] M. Feingold, S. Fishman, D.R. Grempel and R.E. Prange, Phys. Rev. B (Rapid Communications) **31**, 6852 (1985); M. Feingold and S. Fishman, Physica **25D**, 181-195 (1987). M. Feingold, S. Fishman, D.R. Grempel and R.E. Prange, (Comment) in Phys. Rev. Lett. **61**, 377 (1988).
- [19] S.-J. Chang and K.-J. Shi, Phys. Rev. A. **34**, 7 (1986).
- [20] F.M. Izraelev, Phys. Rep. **196**, 299 (1990).
- [21] K. Vant, G. Ball, H. Ammann, and N. Christensen, Phys. Rev. E **59**, 2846 (1999).
- [22] E. Ott, 'Chaos in dynamical systems', Cambridge University Press (1993).
- [23] T. Geisel, G. Radons, and J. Rubner, Phys. Rev. Lett. **57**, 2883 (1986).
- [24] S. Fishman, D.R. Grempel, and R.E. Prange, Phys. Rev. A.**36**, 289 (1987).
- [25] N.T. Maitra and E.J. Heller, Phys. Rev. E. **61**, 3620 (2000).
- [26] C. Mejia-Monasterio, G. Benenti, G.G. Carlo, and G. Casati, quant-ph/0410246 (2004).
- [27] M.V. Berry and M. Robnik, J.Phys.A, **17** , 669 (1986).
- [28] M. Stocklin, PhD thesis, (2006), in preparation.
- [29] T. Dittrich and U. Smilanski, in "Quantum chaos: between order and disorder", 605, Cambridge University Press, Eds G. Casati and B. Chirikov, 1995.